Translational Science

Cancer Research

MDM2 and MDM4 Are Therapeutic Vulnerabilities in Malignant Rhabdoid Tumors

Thomas P. Howard[1,2,3,4], Taylor E. Arnoff[1,2], Melinda R. Song[1,2], Andrew O. Giacomelli[2,3], Xiaofeng Wang[1], Andrew L. Hong[1,2,3], Neekesh V. Dharia[1,3], Su Wang[5], Francisca Vazquez[3], Minh-Tam Pham[1,2], Ann M. Morgan[1,4,6], Franziska Wachter[1,6], Gregory H. Bird[1,6], Guillaume Kugener[3], Elaine M. Oberlick[1,3], Matthew G. Rees[3], Hong L. Tiv[7], Justin H. Hwang[2,3], Katherine H. Walsh[1,3], April Cook[1,2,3], John M. Krill-Burger[3], Aviad Tsherniak[3], Prafulla C. Gokhale[7], Peter J. Park[5], Kimberly Stegmaier[1,3,4], Loren D. Walensky[1,4,6], William C. Hahn[2,3,4], and Charles W.M. Roberts[1,3,4,8]

Abstract

Malignant rhabdoid tumors (MRT) are highly aggressive pediatric cancers that respond poorly to current therapies. In this study, we screened several MRT cell lines with large-scale RNAi, CRISPR-Cas9, and small-molecule libraries to identify potential drug targets specific for these cancers. We discovered *MDM2* and *MDM4*, the canonical negative regulators of p53, as significant vulnerabilities. Using two compounds currently in clinical development, idasanutlin (MDM2-specific) and ATSP-7041 (MDM2/4-dual), we show that MRT cells were more sensitive than other p53 wild-type cancer cell lines to inhibition of MDM2 alone as well as dual inhibition of MDM2/4. These compounds caused significant upregulation of the p53 pathway in MRT cells, and sensitivity was ablated by CRISPR-Cas9–mediated inactivation of *TP53*. We show that loss of SMARCB1, a subunit of the SWI/SNF (BAF) complex mutated in nearly all MRTs, sensitized cells to MDM2 and MDM2/4 inhibition by enhancing p53-mediated apoptosis. Both MDM2 and MDM2/4 inhibition slowed MRT xenograft growth *in vivo*, with a 5-day idasanutlin pulse causing marked regression of all xenografts, including durable complete responses in 50% of mice. Together, these studies identify a genetic connection between mutations in the SWI/SNF chromatin-remodeling complex and the tumor suppressor gene *TP53* and provide preclinical evidence to support the targeting of MDM2 and MDM4 in this often-fatal pediatric cancer.

Significance: This study identifies two targets, MDM2 and MDM4, as vulnerabilities in a deadly pediatric cancer and provides preclinical evidence that compounds inhibiting these proteins have therapeutic potential.

Introduction

Malignant rhabdoid tumors (MRT) are highly aggressive cancers associated with extremely poor prognoses despite intensive therapy (1–3). MRTs typically arise in young children in the kidney, brain (atypical teratoid/rhabdoid tumors, ATRT), and soft tissues (4). Irrespective of location, nearly all MRTs are defined by genetic inactivation of *SMARCB1/SNF5/INI1/BAF47*, a core subunit of the SWI/SNF (BAF) chromatin-remodeling complex (4). Other than loss of SMARCB1, MRTs contain remarkably simple genomes with no other recurrent mutations detected (5–8). *SMARCB1* possesses bona fide tumor-suppressive activity, as conditional inactivation of the gene in mice results in the rapid onset of fully penetrant cancer at a median of only 11 weeks (9). Nevertheless, the mechanisms by which SMARCB1 loss promotes cancer remain poorly understood. Current research has implicated widespread enhancer dysregulation (10, 11) arising from disruption of antagonism with other epigenetic regulators (12–14) and resulting in transcriptional changes in a number of cancer-related pathways as contributors to the tumor-suppressive function of SMARCB1 (15).

MRTs lack a clear therapeutically targetable oncogenic lesion because the sole recurrent mutation is inactivation of *SMARCB1*. Consequently, we searched for synthetic lethal relationships by performing genome-scale RNAi and CRISPR-Cas9 screens as well as a large small-molecule screen. We show that *MDM2* and *MDM4* are vulnerabilities in MRTs. MDM2 is an E3 ubiquitin ligase that targets p53 for proteasomal degradation while MDM4 (MDMX) binds and sequesters p53, thus blocking p53 transcriptional

[1]Department of Pediatric Oncology, Dana-Farber Cancer Institute and Division of Hematology/Oncology, Boston Children's Hospital, Boston, Massachusetts. [2]Department of Medical Oncology, Dana-Farber Cancer Institute, Boston, Massachusetts. [3]Broad Institute of Harvard and MIT, Cambridge, Massachusetts. [4]Harvard Medical School, Boston, Massachusetts. [5]Department of Biomedical Informatics, Harvard Medical School, Boston, Massachusetts. [6]Linde Program in Cancer Chemical Biology, Dana-Farber Cancer Institute, Boston, Massachusetts. [7]Experimental Therapeutics Core and Belfer Center for Applied Cancer Science, Dana-Farber Cancer Institute, Boston, Massachusetts. [8]Department of Oncology, Comprehensive Cancer Center, St. Jude Children's Research Hospital, Memphis, Tennessee.

Note: Supplementary data for this article are available at Cancer Research Online (http://cancerres.aacrjournals.org/).

Corresponding Authors: Charles W.M. Roberts, St. Jude Children's Research Hospital, Mail Stop 281, 262 Danny Thomas Place, Memphis, TN 38105-3678. Phone: 901-595-3913; Fax: 901-595-7478; E-mail: Charles.roberts@stjude.org; and William C. Hahn, Dana-Farber Cancer Institute, 450 Brookline Avenue, D1538, Boston, MA 02215. Phone: 617-632-2641; E-mail: william_hahn@dfci.harvard.edu

doi: 10.1158/0008-5472.CAN-18-3066

activity by two distinct mechanisms (16). MDM2 and MDM4 can also form heterodimers that are more active than their respective homodimers (17). We noted that MRT cells, due to loss of SMARCB1, are more sensitive to MDM2 and dual MDM2/4 inhibition than other p53 wild-type cancer cell lines. Targeting of MDM2 also showed a dramatic inhibitory effect on the growth of MRT xenografts. Together, these studies nominate new treatments for this highly deadly disease while building further understanding of how the SWI/SNF complex may influence the transcriptional activity of p53.

Materials and Methods

Cell lines

Cell lines were obtained from the ATCC (A204, A549, G401, G402, HCT116, HEYA8, JEG3, SAOS2, SJSA1, SW480, U2OS), Yoon-Jae Cho (ATRT3), C. David James (BT12, BT16), Children's Oncology Group (CHLA266, COGAR359), Yasumichi Kuwahara (DL, KPMRTRY), JCRB Cell Bank (JMURTK2), Frank Bourdeaut (KD, MON), Broad Institute Biological Samples Platform (KYM1), Bernard Weissman (NCIH2004RT, TM87), Geoffrey Wahl (SJSAX), and Tim Triche (STM9101, TTC1240, TTC549, TTC642, TTC709). Growth conditions are described in Supplementary Table S1. All lines were SNP authenticated prior to screening, and were *Mycoplasma*-tested after freezing stocks, before screening, and before *in vivo* experiments.

Project Achilles RNAi and CRISPR-Cas9 screens

We analyzed a published genome-scale RNAi screen of 501 cancer cell lines (10 MRTs; ref. 18) and an updated version of the GeCKOv2 CRISPR-Cas9 screen of 43 cancer cell lines (8 MRTs; refs. 19, 20). The CRISPR-Cas9 data used in this manuscript (DepMap GeCKO 19Q1) can be downloaded from the Figshare repository (DOI: dx.doi.org/10.6084/m9.figshare.7668407). For cell line p53 status annotations, we adapted a published protocol (21). Classifications are detailed in Supplementary Table S2. Further information on analysis is available in the Supplementary Methods.

Cancer therapeutics response portal analysis

We analyzed data from cancer therapeutics response portal (CTRP) v2 (22, 23), which contained area under the curve (AUC) from 16-point dose curves for 860 cell lines and 481 small molecules. We compared the sensitivity to nutlin-3 of MRT cell lines ($n = 9$) with all other adherent cell lines ($n = 467$).

In vitro sensitivity

For dose curves, cells were treated for 72 hours with idasanutlin (MedChemExpress, catalog no. HY-15676; nine-point half-log curve from 50 μmol/L to 5 nmol/L at 0.5% DMSO) or ATSP-7041 [synthesized as published (24, 25); seven-point three-fold curve from 30 μmol/L to 41 nmol/L at 0.3% DMSO]. CellTiter-Glo (Promega, catalog no. G7573) was added and plates read on an EnVision 2103 (PerkinElmer) or SpectraMax M5e (Molecular Devices). Three technical replicates at each concentration were averaged and normalized to DMSO. The average of normalized values from 3–4 biological replicates were plotted on GraphPad Prism, and IC_{50} values calculated with the log[inhibitor] – variable slope function. For further information, please see our protocols.io entry (DOI: dx.doi.org/10.17504/protocols.io.whyfb7w).

For counting, cells were treated with idasanutlin (1 μmol/L), ATSP-7041 (5 μmol/L), or DMSO (0.05%) for 24, 48, and 72 hours, and counted using a Vi-CELL XR Cell Viability Analyzer (Beckman Coulter). Counts from three technical replicates were averaged, normalized to 0 hours, transformed to a $\log_2$ scale, and the mean and SD of three biological replicates calculated. For further information, please see our protocols.io entry (DOI: dx.doi.org/10.17504/protocols.io.wh4fb8w).

For β-galactosidase staining, cells were treated for 72 hours as above, replated at equal densities for 4-day recovery, and stained using the Senescence β-Galactosidase Staining Kit (Cell Signaling Technology #9860S). Fifteen images (200×) for each condition were deidentified, randomized, scored, summed, and the percentage of β-galactosidase–positive cells calculated. Finally, the mean and SD from three biological replicates was computed. For further information, please see our protocols.io entry (DOI: dx.doi.org/10.17504/protocols.io.widfca6).

For colony formation, cells were treated for 72 hours as above and replated at equal low densities for 7-day recovery. Cells were fixed in methanol and stained with crystal violet solution (0.5% w/v crystal violet, 25% methanol). For quantitation, crystal violet was extracted with 10% acetic acid, read on a SpectraMax M5e at 595 nm, and technical triplicates were averaged. The mean and SD from three biological replicates was computed. For further information, please see our protocols.io entry (DOI: dx.doi.org/10.17504/protocols.io.wiefcbe).

p53-null clone generation

We attempted to delete the DNA-binding domain of *TP53* with two sgRNAs [Supplementary Table S3; designed with E-CRISP (26)] targeting exons 4 and 9 using a previously described method (27). Clones were grown and screened for *TP53* deletion by PCR (Supplementary Table S4) followed by immunoblot for absence of p53 protein. *TP53*-null clones were then characterized by immunoblot, qRT-PCR, and PCR followed by Sanger sequencing (Supplementary Table S4). For further information, please see our protocols.io entry (DOI: dx.doi.org/10.17504/protocols.io.wh2fb8e).

Immunoblots

Cell pellets or homogenized tumors were lysed in 1× RIPA Buffer (Millipore Sigma, catalog no. 20-188) containing 1× Protease/Phosphatase Inhibitor Cocktail (Cell Signaling Technology, catalog no. 5872S) and quantitated using the Pierce BCA Protein Assay Kit (Thermo Fisher Scientific, catalog no. PI23225). Protein was then denatured in 1× NuPAGE LDS Sample Buffer (Thermo Fisher Scientific, catalog no. NP0007) with 5% β-mercaptoethanol and equal amounts (5–20 μg) electrophoresed in NuPAGE 4%–12% Bis-Tris Protein Gels (Thermo Fisher Scientific). Proteins were transferred to nitrocellulose membranes using the iBlot System (Thermo Fisher Scientific) and incubated in Odyssey Blocking Buffer (PBS; LI-COR, catalog no. 927-40010). Membranes were cut as necessary and incubated in primary antibodies (Supplementary Table S5) overnight at 4°C followed by fluorescent secondary antibodies (LI-COR) for 1 hour. Membranes were washed in PBS-T and scanned using an Odyssey Imaging System (LI-COR). For further information, please see our protocols.io entry (DOI: dx.doi.org/10.17504/protocols.io.whkfb4w).

qRT-PCR

Cells were harvested and RNA extracted from TRIzol reagent (Thermo Fisher Scientific, catalog no. 15596026). A total of 2 μg of RNA was reverse transcribed into cDNA using SuperScript VILO Master Mix (Thermo Fisher Scientific, catalog no. 11755050). qRT-PCR reactions consisted of 1× Power SYBR Green PCR Master Mix (Thermo Fisher Scientific, catalog no. 4368708), 500 nmol/L each primer (Supplementary Table S4), and 5 ng cDNA in triplicate. Plates were run on the ViiA 7 Real-Time PCR System (Thermo Fisher Scientific). Relative gene expressions were calculated using a $\Delta\Delta C_t$ method compared with an internal GAPDH control, and the relative expression levels of three biological replicates averaged. For further information, please see our protocols.io entry (DOI: dx.doi.org/10.17504/protocols.io.wh3fb8n).

RNA-sequencing

TTC642 cells were treated with idasanutlin (1 μmol/L) or DMSO (0.01%) for 24 hours in biological triplicates. RNA was isolated using TRIzol as above and purified using an RNeasy MinElute Cleanup Kit (Qiagen, catalog no. 74204). Libraries were prepared from 1 μg of RNA using the NEBNext Ultra RNA Library Prep Kit for Illumina (New England BioLabs, catalog no. E7530S) with NEBNext Multiplex Oligos for Illumina (New England BioLabs, catalog no. E7335S) with 12 cycles of amplification. Library quality was assessed using an Agilent 2200 Tapestation System (Agilent Technologies) and quantified using a Qubit 4 Fluorometer (Thermo Fisher Scientific). Equal molar amounts were pooled, diluted, denatured, and sequenced on a NextSeq500 (Illumina). Fastq files have been deposited to the Gene Expression Omnibus (GSE124508). Further information on data analysis is available in the Supplementary Methods.

Flow cytometry

For cell cycle, cells were treated with idasanutlin (1 μmol/L), ATSP-7041 (5 μmol/L), or DMSO (0.05%) for 24 hours, fixed in 70% ethanol, and stained with FxCycle Propidium Iodide (PI)/RNase Staining Solution (Thermo Fisher Scientific, catalog no. F10797). Cells were run on an SA3800 Spectral Analyzer (Sony). PI histogram distributions were analyzed using ModFit LT Version 5. The difference in percentage of G_0–G_1 cells compared with DMSO was computed, and three biological replicates averaged.

For apoptosis, cells were treated as above and stained with the BD Annexin V: FITC Apoptosis Detection Kit I (Thermo Fisher Scientific, catalog no. BDB556547). Cells were run on an SA3800 Spectral Analyzer, and its software used to unmix the PI and FITC signals. Samples were then analyzed in FlowJo 10.

For further information, please see our protocols.io entry (DOI: dx.doi.org/10.17504/protocols.io.whjfb4n).

SMARCB1 and p16^{INK4A} expression

A *SMARCB1* variant 2 ORF was obtained from the Human ORFeome 8.1 and cloned into pLX401 (David Root; Addgene, catalog no. 41393) to create pLX401-SMARCB1 (Addgene, catalog no. 111182). A codon-optimized p16^{INK4A} ORF was synthesized (Integrated DNA Technologies) and cloned to produce pLX401-INK4A (Addgene, catalog no. 121919). Following lentiviral transduction and selection, gene expression was induced by 1 μg/mL doxycycline (Clontech, catalog no. NC0424034) 48 hours prior to assays to allow for sufficient protein expression and SMARCB1 inclusion into the SWI/SNF complex (10). For dose curves, cells were treated for an additional 72 hours, while for immunoblots, qRT-PCR, and flow cytometry, cells were treated for an additional 24 hours. For further information, please see our protocols.io entry (DOI: dx.doi.org/10.17504/protocols.io.wiffcbn).

Xenografts

All *in vivo* studies were performed under approved protocols of the Dana-Farber Cancer Institute's Institutional Animal Care and Use Committee.

For all experiments, 2×10^6 cells in 100 μL [1:1 PBS:Matrigel (Corning, catalog no. 354234)] were injected subcutaneously into 6–8 week-old female NCr Nude mice (Taconic, catalog no. NCRNU-F). To test tumor formation capacities, both flanks of 4 mice were used. Caliper measurements (volume = length*width^2/2) were taken twice per week for 2 weeks and then once per week. Endpoints were as follows: (i) total volume >2,000 mm^3 or (ii) total length >20 mm.

For efficacy studies, TTC642 cells were injected into the right flank as above. When tumors reached approximately 150–250 mm^3, mice were randomized [stratified randomization; Study Director 3.1 (Studylog)] to vehicle, idasanutlin, or ATSP-7041 (n = 8/arm). Vehicle and idasanutlin were dosed at 150 mg/kg orally twice per day for 5 days. ATSP-7041 was dosed at 30 mg/kg by tail vein injection every other day for 20 days. Tumor volumes and body weights were measured twice per week for 8 weeks, followed by once per week. Endpoints were as follows: (i) total volume >2,000 mm^3; or (ii) 100 days following randomization.

For pharmacodynamics studies, TTC642 cells were injected, randomized (n = 3/arm), and given 5 doses as above. Mice were euthanized 2 hours (vehicle and idasanutlin) or 4 hours (ATSP-7041; longer stapled peptide uptake time) following the final treatment. Tumors were divided and snap-frozen or fixed in formalin.

Idasanutlin (50% w/w idasanutlin/pharmaceutical polymer) and vehicle were provided by Roche. The vehicle was composed of 2% w/w hydroxyl propyl cellulose, 0.1% w/w polysorbate 80, 0.09% methyl paraben, 0.01% propyl paraben, 0.0072% sodium acetate, and 0.0569% glacial acetic acid. Idasanutlin was resuspended in vehicle to 15 mg/mL (dose = 10 mL/kg). ATSP-7041 was formulated for *in vivo* studies as reported (28).

IHC of xenografts

Fixed tumors were trimmed, cassetted, embedded, and mounted using standard protocols at the DF/HCC Rodent Histopathology Core. Slides were stained for Ki-67 IHC (Supplementary Table S5) at the DF/HCC Specialized Histopathology Core. Representative images of >1,000 cells/tumor were deidentified, randomized, and scored for the percentage of Ki-67$^+$ cells. Three tumors per arm were averaged.

Primary tumor expression analysis

Primary MRT samples were profiled using RNA-sequencing through the NCI Therapeutically Applicable Research to Generate Effective Treatments (TARGET) initiative (http://ocg.cancer.gov/programs/target; ref. 29). Additional TARGET TPM expression data for other pediatric cancers were downloaded through UCSC Xena (http://xena.ucsc.edu, TARGET Pan-Cancer (PANCAN) dataset). The 13-gene expression signature for predicting sensitivity to MDM2 inhibition was adapted from (30). Further information on analysis is available in the Supplementary Methods.

Results

To identify potential drug targets for MRTs, we screened MRT cell lines as part of Project Achilles (18, 20) with pooled-format RNAi ($n = 10$) and CRISPR-Cas9 ($n = 8$) screens. The RNAi screens implicated regulation of the p53 pathway, as *MDM4* suppression resulted in the largest preferential proliferation deficit in MRT cells of all genes tested, while *TP53* suppression caused a highly significant survival advantage (Supplementary Fig. S1A). We consequently evaluated the p53 pathway in the CRISPR-Cas9 screens, and found inactivation of *MDM2* to be the strongest vulnerability and inactivation of *TP53* to cause the most significant enrichment (Fig. 1A). *MDM4*, in addition to two other negative regulators of p53, *PPM1D* and *USP7*, also scored among the top vulnerabilities in the CRISPR-Cas9 screen, while other p53-related tumor suppressors scored as genes that were significantly enriched in SMARCB1-deficient cells (Fig. 1A). Together, these observations suggest that MRT cells proactively suppress an otherwise functional p53 pathway to achieve a survival advantage.

We then asked whether MRT lines, which retain wild-type (WT) *TP53* and functional p53 pathways (31), were more sensitive to perturbations of the p53 pathway than other p53 WT cell lines. Indeed, MRT cells were significantly more vulnerable to Cas9-mediated genetic inactivation of three of four negative regulators of p53 (*MDM2:* $P = 0.027$; *PPM1D:* $P = 0.0045$; *USP7:* $P = 0.016$), and the survival advantage conferred through inactivation of *TP53* was considerably larger ($P < 0.0001$; Supplementary Fig. S1B–S1F). Given this particular dependence on *MDM2*, we investigated whether MRT cell lines were more sensitive to nutlin-3, a canonical MDM2 inhibitor, than other cancer cell lines in a large-scale small-molecule sensitivity dataset [Cancer Therapeutics Response Portal (CTRP); refs. 22, 23]. Indeed, MRT cell lines ($n = 9$) were significantly more sensitive than all other adherent cancer cell lines ($P < 0.0001$; Fig. 1B) and other p53 WT adherent cell lines ($P = 0.0004$; Fig. 1C). Overall, these findings suggest that specific properties of MRT cells beyond maintaining WT *TP53* contribute to their sensitivity to p53 pathway manipulation.

We next evaluated idasanutlin (RG7388; ref. 32), a small-molecule inhibitor of MDM2 that has entered clinical trials for blood and solid tumors (NCT02545283, NCT03362723, others), and ATSP-7041 (25), a prototype stapled peptide inhibitor of both MDM2 and MDM4 related to ALRN-6924, which is in clinical trials for multiple cancer types (NCT02264613, NCT02909972). We found that MRT cells were significantly more sensitive to both idasanutlin ($P = 0.015$) and ATSP-7041 ($P = 0.0014$) than other p53 WT cancer cells (Fig. 2A–D). The most sensitive MRT cell lines were comparably sensitive to MDM2-amplified SJSA1 osteosarcoma cells, often used as a positive control for MDM2 inhibition [Fig. 2A and C; CCLE (33)]. Consistent with the observed differential activity of these compounds, idasanutlin was least active against MDM4 overexpressing cancer cells (JEG3, SJSAX), whereas these same cells were among the more responsive lines to ATSP-7041 treatment. In addition, BT12, the least sensitive MRT line to nutlin-3 and idasanutlin, is the only MRT line that harbors a deletion of *CDKN2A*, likely leading to increased MDM2 activation and explaining its relative resistance to the inhibitors. MRTs arising in different organs were similarly sensitive (Supplementary Fig. S2A and S2B). MRT cell lines did not express more MDM2 or MDM4 than other p53 WT cell lines (Supplementary Fig. S2C–S2E), which was consistent with a previous report that primary MRT samples did not express high levels of MDM2 (34). These observations indicate that both the

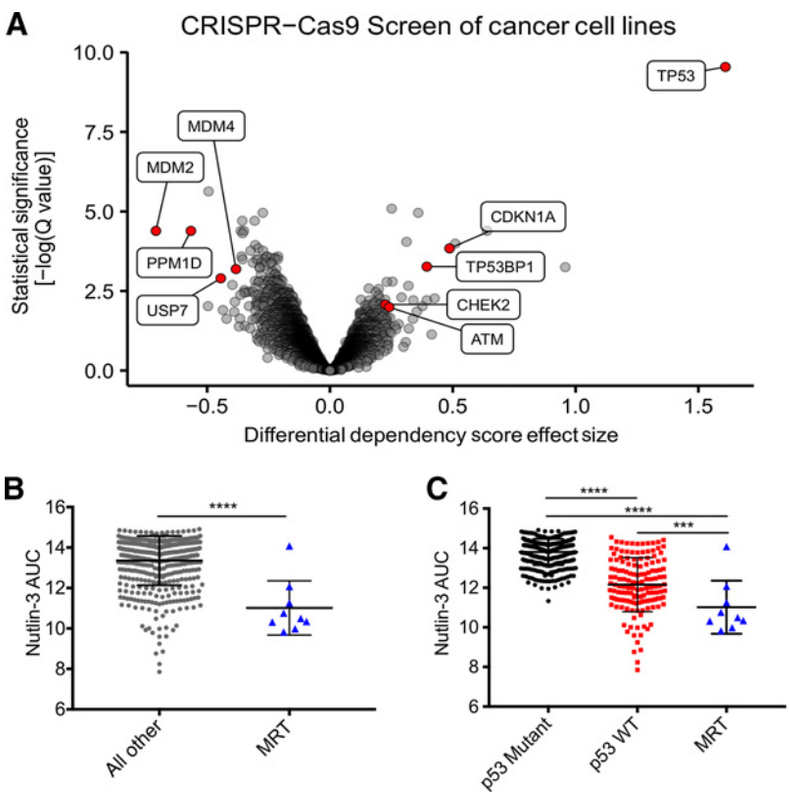

Figure 1.

Large-scale screens identify *MDM2* and *MDM4* as vulnerabilities in MRTs. **A,** Genome-scale CRISPR-Cas9 screens of 43 cancer cell lines (8 MRTs). Each circle represents one gene. The *x*-axis represents the mean difference of dependency scores in MRT cell lines compared with others. Negative dependency scores indicate that MRT cells require that gene, whereas positive scores suggest that the gene suppresses MRT growth. Significance calculated as $-\log_{10}(Q \text{ value})$ from two-sided *t* tests with Benjamini–Hochberg correction. **B,** Sensitivities of 476 cancer cell lines (9 MRTs) to nutlin-3. Each point represents one cell line. AUC calculated from 16-point dose curves. Smaller AUCs indicate greater sensitivity. Data show mean ± SD. Significance calculated by a two-sided *t* test. **C,** Replot of **B**, segregating cell lines by p53 status. Significance calculated by one-way ANOVA with Holm–Sidak correction. ***, $P < 0.001$; ****, $P < 0.0001$.

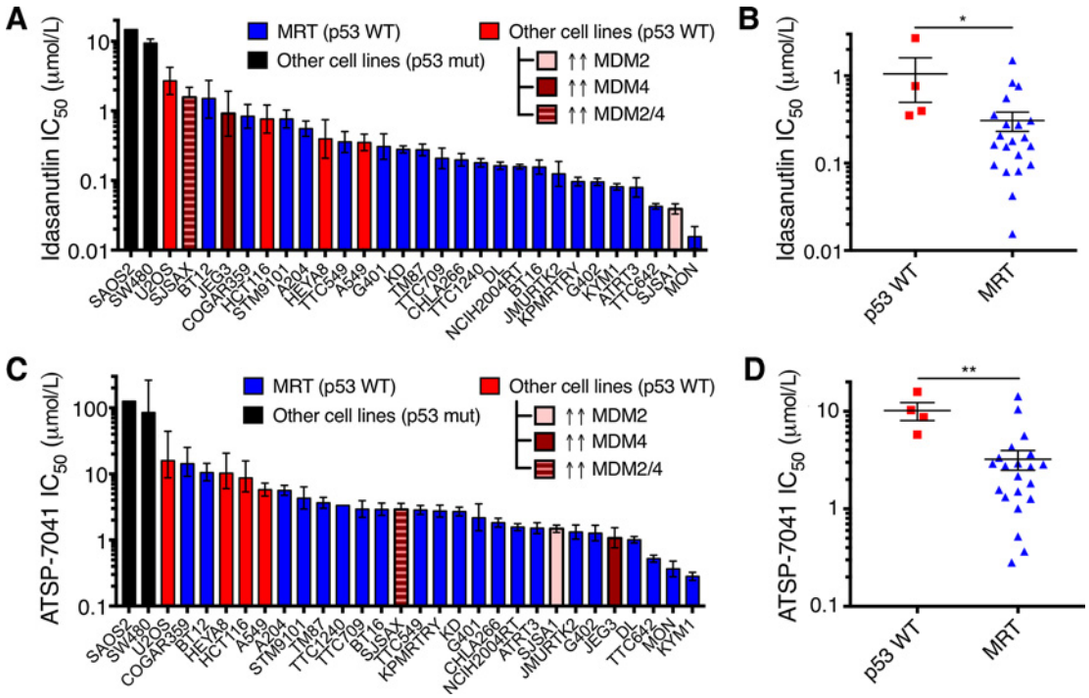

Figure 2.

MRT cell lines are more sensitive to MDM2 and MDM2/4 inhibition than other p53 wild-type cell lines. **A,** IC_{50} for idasanutlin in cell lines calculated from dose response curves. Controls include p53 WT cells, a subset with amplification/overexpression of MDM2/4. Data show mean ± 95% CI from three biological replicates. **B,** IC_{50} of p53 WT, non-MDM2/4 amplified cell lines, and MRT cells. Each point represents one cell line from **A**. Data show mean ± SEM. Significance calculated by a two-sided *t* test. **C** and **D,** IC_{50} for ATSP-7041 in cell lines, as plotted in **A** and **B**. *, $P < 0.05$; **, $P < 0.01$.

small-molecule MDM2 and stapled peptide MDM2/4 inhibitors decrease the proliferation of MRT cells more effectively than other p53 WT cell lines, and this greater sensitivity is not due to differential expression of MDM2/4.

To confirm that the observed findings were due to on-target effects on the p53 pathway, we inactivated *TP53* using CRISPR-Cas9 in two MRT cell lines and characterized a number of p53-null clones (Supplementary Fig. S3A–S3E). These clones were indeed resistant ($P < 0.0001$) to both idasanutlin and ATSP-7041 (Fig. 3A–D). Then, we treated MRT and control cell lines with idasanutlin and ATSP-7041 at concentrations at which the p53-null cells were unaffected by treatment and assayed the p53 pathway by immunoblot. All MRT lines tested accumulated p53 and upregulated canonical p53 target genes *p21* and *MDM2*, while the p53-null clones did not (Supplementary Fig. S4A–S4B). To characterize gene expression changes caused by MDM2 inhibition in MRTs, we performed RNA-seq on TTC642 cells treated with idasanutlin. When compared with DMSO, idasanutlin treatment caused significant upregulation of 89% of high-confidence p53 target genes (Fig. 3E; Supplementary Table S6; ref. 35). In addition, when we performed gene set enrichment analysis (36), we found that the p53 signaling pathway was the most strongly represented gene set (Supplementary Table S7). Together, these experiments confirm that idasanutlin and ATSP-7041 activate the p53 pathway in MRT cell lines and that MRT sensitivity to these compounds is due to on-target effects on the p53 pathway.

Because p53 activation can lead to disparate cell fate decisions (cell-cycle arrest, senescence, or apoptosis) in different contexts, we investigated how MRT cell lines respond to MDM2 or MDM2/4 inhibition. Of the four cell lines tested, the three most sensitive lines (G402, MON, TTC642) showed substantial decreases in cell number when treated with either compound (Supplementary Fig. S5A–S5C). Two of these cell lines (G402, TTC642) underwent a combination of cell-cycle arrest (Supplementary Fig. S5D) and apoptosis, as evidenced by increased cleaved caspase-3 (Supplementary Fig. S4A and S4B) and Annexin V staining (Supplementary Fig. S5E–S5J). Furthermore, *TP53I3*, a well-characterized apoptotic mediator, was the most significantly upregulated p53 target gene in TTC642 cells upon idasanutlin treatment (Fig. 3E; Supplementary Table S6). In addition, the least sensitive MRT cell line tested (G401) stopped proliferating (Supplementary Fig. S5K). This cytostatic response corresponded with significant increases in senescence-associated β-galactosidase staining with both idasanutlin ($P = 0.0044$) and ATSP-7041 ($P = 0.0014$) treatment (Supplementary Fig. S5L and S5M), with a majority of cells failing to resume proliferation following removal of treatment (Supplementary Fig. S5N and S5O). These findings indicate that MRT cells primarily respond to MDM2 and MDM2/4 inhibition with permanent apoptotic or senescent cell fate decisions.

Because we found that MRT cells are more sensitive to MDM2 and MDM2/4 inhibitors than other p53 WT cells, we hypothesized that loss of *SMARCB1*, the defining mutation in MRTs, contributed to this sensitivity. To test this hypothesis, we expressed SMARCB1 using a doxycycline-inducible construct in three different MRT cell lines. In all cases, SMARCB1 expression led to a modest but significant ($P < 0.0001 – 0.0003$) resistance to

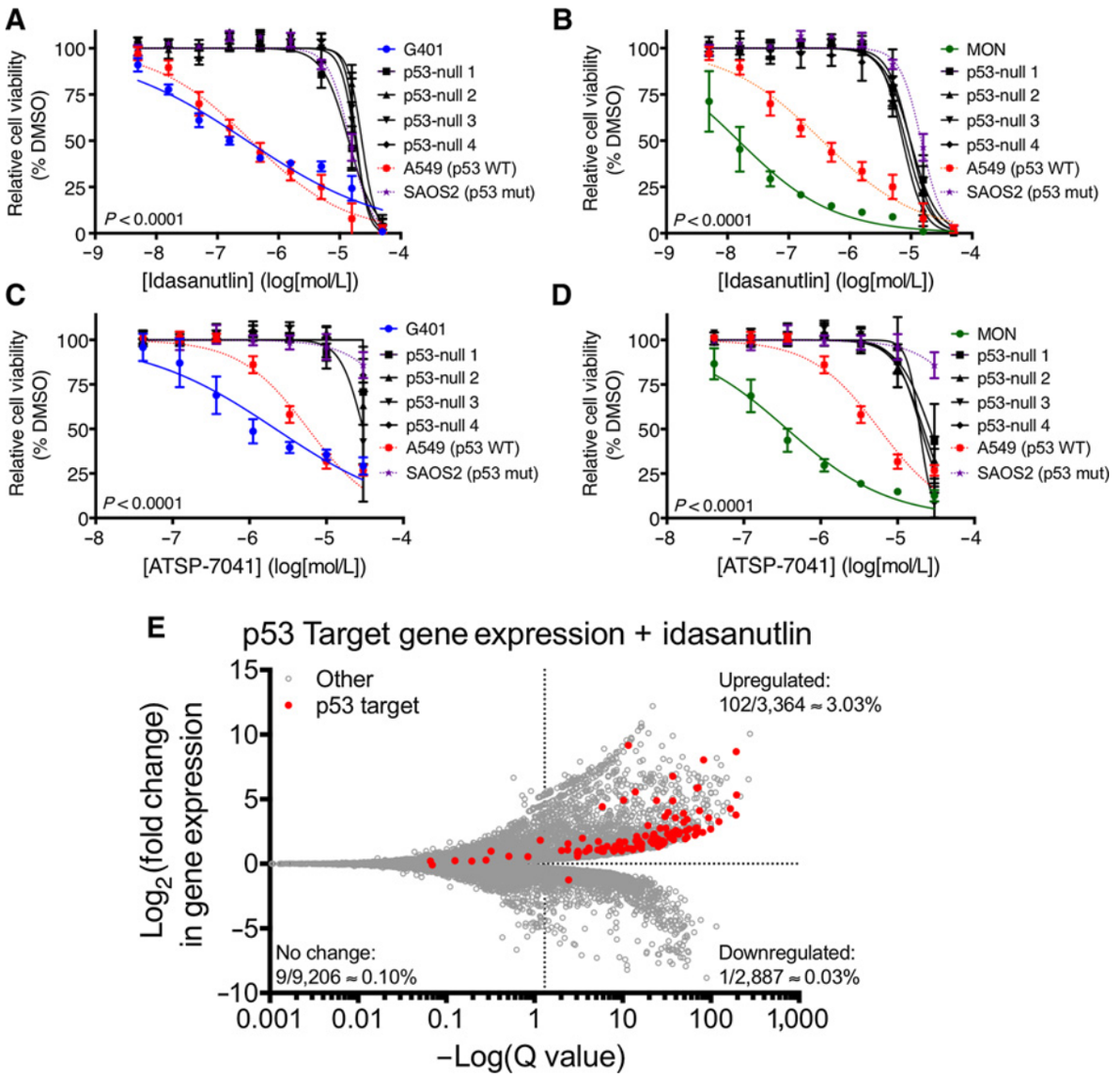

Figure 3.

MRT cell lines demonstrate on-target, p53-dependent sensitivity to MDM2 and MDM2/4 inhibition. **A–D,** Sensitivity of p53-null clones of G401 (**A** and **C**) and MON (**B** and **D**) MRT cell lines to idasanutlin (**A** and **B**) and ATSP-7041 (**C** and **D**). G401, MON, A549, and SAOS2 curves as in Fig. 2. Data show mean ± SD of three biological replicates. Significance between parental and p53-null clones calculated using extra-sum-of-squares F test. **E,** RNA-seq data for all genes (gray) and high confidence p53 targets (red) in TTC642 MRT cells treated with idasanutlin (1 μmol/L for 24 hours) compared with DMSO. Points right of the vertical dash are significant ($Q < 0.05$). For each section, the percentage of total genes that are direct p53 targets is indicated.

idasanutlin and ATSP-7041 (Fig. 4A–G), suggesting that mutation in *SMARCB1* enhances vulnerability to these inhibitors.

Next, we assessed whether the p53 pathway was activated by idasanutlin to the same extent in MRT cells that reexpressed SMARCB1. At both the protein and RNA levels, less p53 accumulated upon idasanutlin treatment when SMARCB1 was reexpressed (Fig. 5A and B). Notably, the increase in p21 (*CDKN1A*) following idasanutlin treatment was comparable at the protein and RNA levels irrespective of the SMARCB1 status (Fig. 5A and C). However, the p53-mediated transcription of *BBC3* and *TP53I3*, two key proapoptotic mediators, was significantly dampened (*BBC3:* $P = 0.028$; *TP53I3:* $P = 0.0019$) when SMARCB1 was reexpressed (Fig. 5D and E). Most strikingly, the increase in cleaved caspase-3 observed with idasanutlin treatment was eliminated by expression of SMARCB1 (Fig. 5A). In addition, SMARCB1 expression partially rescued the observed increases in Annexin V staining upon inhibitor treatment (Supplementary Fig. S5H–S5J and S6A–S6C). To confirm that these data were not merely due to changes in proliferation rates upon SMARCB1 reexpression, we also overexpressed $p16^{INK4A}$ in TTC642 cells. Although $p16^{INK4A}$ similarly decreased cell proliferation (Supplementary Fig. S6D), $p16^{INK4A}$ expression did not impact sensitivity to MDM2 and MDM2/4 inhibition or caspase-3 cleavage (Supplementary Fig. S6E–S6G). Together, these findings suggest

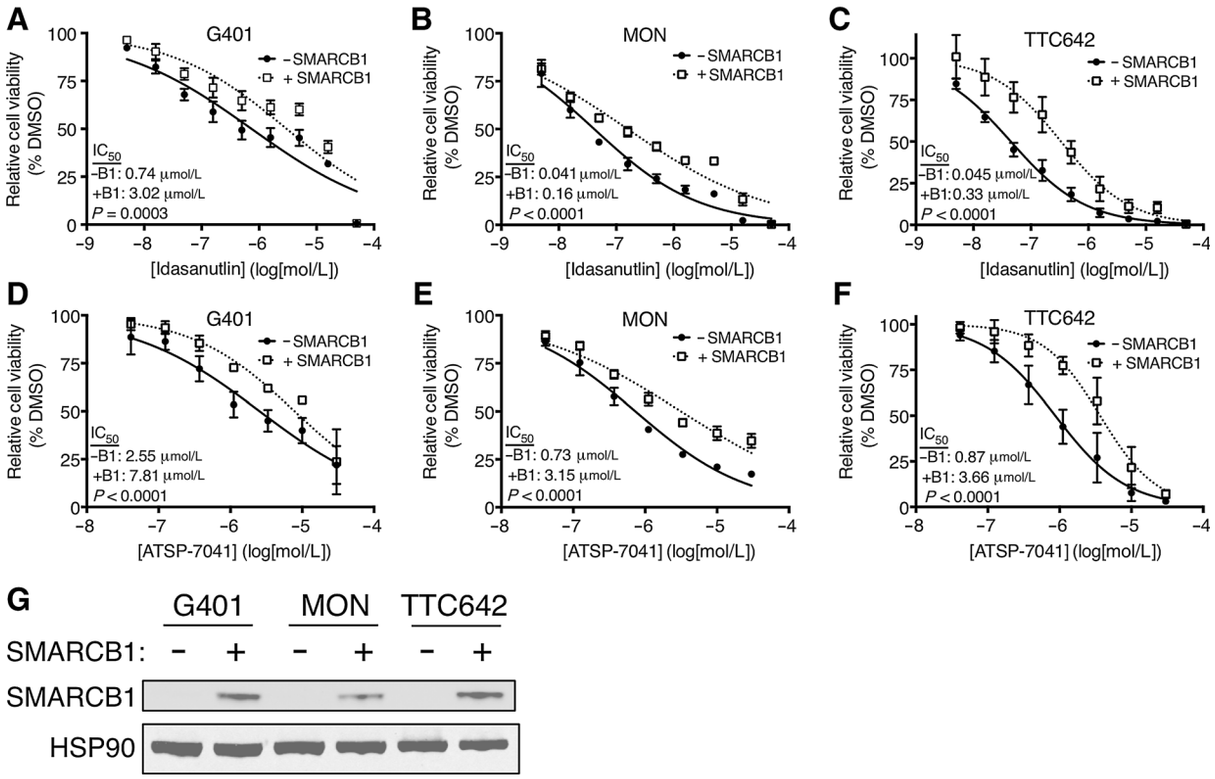

Figure 4.

Gain of SMARCB1 in MRT cells reduces sensitivity to MDM2 and MDM2/4 inhibition. Sensitivity of uninduced and SMARCB1-expressing G401 (**A** and **D**), MON (**B** and **E**), and TTC642 (**C** and **F**) MRT cells to idasanutlin (**A**–**C**) and ATSP-7041 (**D**–**F**). Data show mean ± SD of three biological replicates. Significance calculated using an extra-sum-of-squares F test. **G,** Immunoblot for reexpression of SMARCB1 in MRT cell lines. Representative of three independent replicates.

that the absence of SMARCB1 causes MRT cells to activate p53-mediated apoptosis in response to MDM2 inhibition at levels greater than other p53 WT cells.

We next investigated whether idasanutlin and ATSP-7041 had activity against MRT xenografts *in vivo*. We chose the TTC642 cell line given the rate and consistency with which these cells engrafted

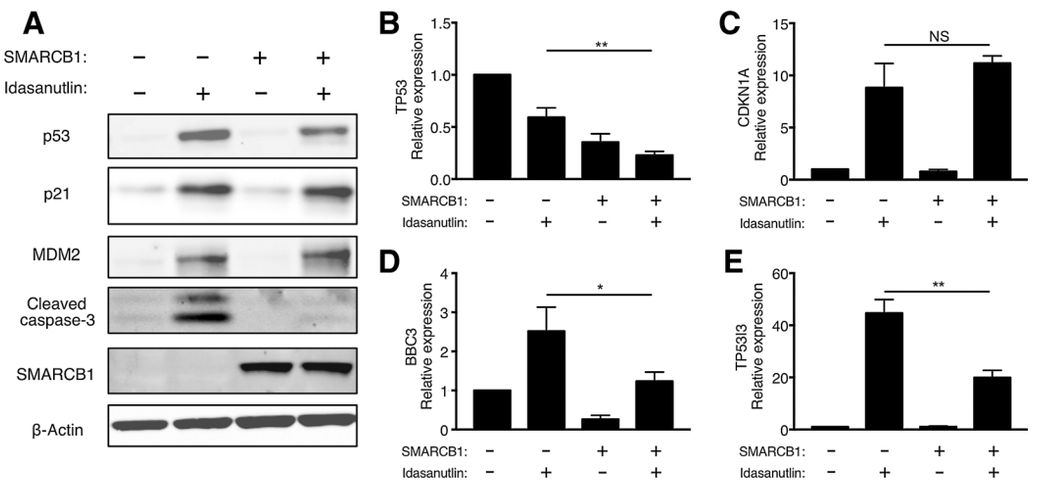

Figure 5.

Gain of SMARCB1 in MRT cells decreases p53-mediated apoptosis. **A,** Immunoblot for p53 pathway responses to idasanutlin treatment (1 μmol/L for 24 hours) in TTC642 cells reexpressing SMARCB1. Images are representative of three biological replicates. **B**–**E,** qRT-PCR for p53 pathway responses to idasanutlin treatment in TTC642 cells reexpressing SMARCB1. Data show relative expression mean ± SD between three biological replicates. Significance calculated by a two-sided *t* test. *, $P < 0.05$; **, $P < 0.01$; ns, nonsignificant.

tumors compared with three other MRT cell lines (Supplementary Fig. S7A–S7D). The small-molecule idasanutlin was administered twice per day orally at 150 mg/kg per dose for 5 days, whereas the stapled peptide ATSP-7041 was dosed at 30 mg/kg/i.v. every other day for 20 days. ATSP-7041 slowed the growth of all tumors ($P < 0.0001$) and significantly extended survival ($P = 0.0022$; Fig. 6A and B). Idasanutlin, meanwhile, caused marked shrinkage of all tumors (Fig. 6A and C; $P < 0.0001$), which resulted in complete and durable responses in 50% of mice (survival: $P = 0.0001$; Fig. 6B and D). The tumors that subsequently grew (4 of 8) did so only 9–12 days after idasanutlin treatment had ceased (Fig. 6D). This response was achieved at doses that did not substantially affect mouse weight (Supplementary Fig. S7E). Both idasanutlin and ATSP-7041 significantly decreased the percentage of proliferating cells as measured by Ki-67 staining (Fig. 6E; Supplementary Fig. S7F–S7H). Treatment with idasanutlin or ATSP-7041 caused substantial upregulation of p21 and MDM2 levels as well as apoptotic induction in tumors, although p53 levels varied (Fig. 6F). Overall, these data strongly support further clinical investigation of small molecules and stapled peptides that reactivate the p53 pathway for MRT treatment.

Finally, we utilized gene expression signatures of primary MRT samples to predict susceptibility to MDM2 inhibition. Higher expression of thirteen p53 target genes was previously shown to predict greater sensitivity to MDM2 inhibition (30). We analyzed gene expression data from 37 primary MRTs of the kidney along with six normal kidney pairs and 656 other pediatric cancers (29).

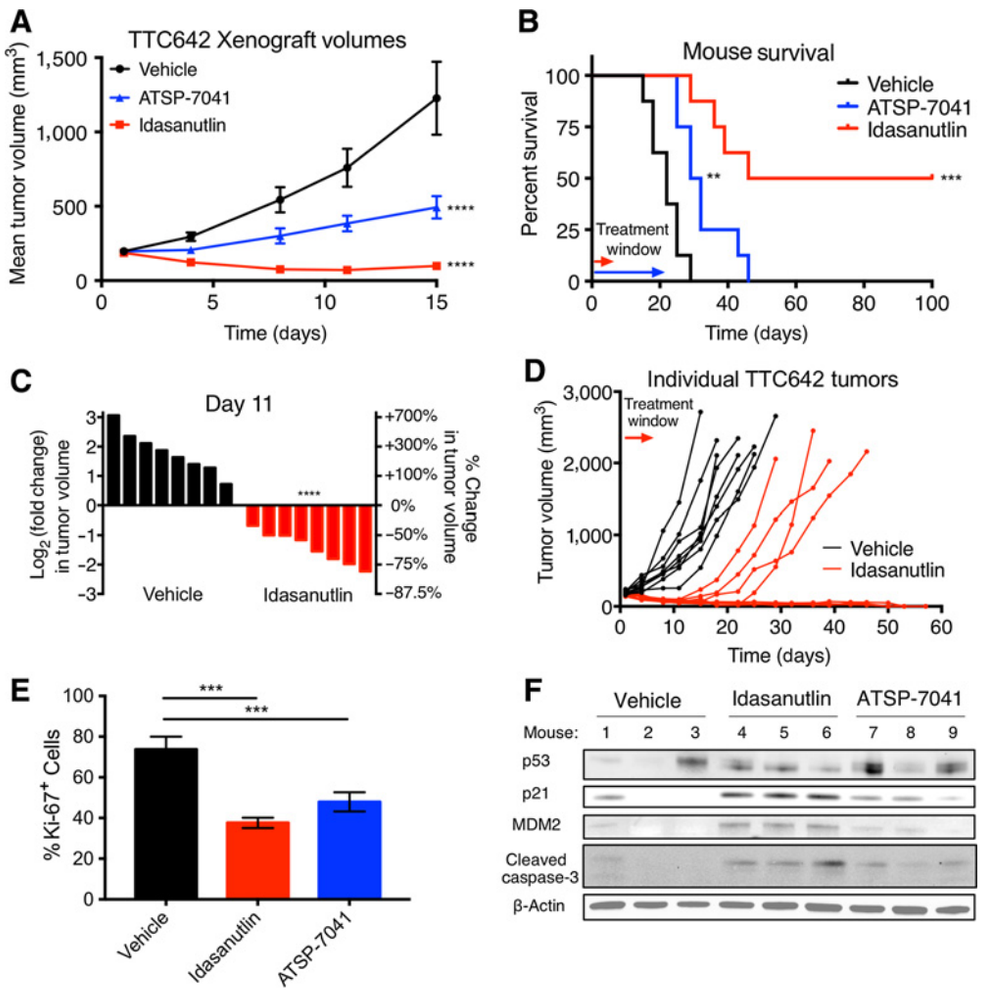

Figure 6.

MDM2 and MDM2/4 inhibition decreases MRT xenograft growth *in vivo*. **A,** Tumor volumes for vehicle, idasanutlin, and ATSP-7041–treated mice. $n = 8$ per group. Data show mean ± SEM. Significance calculated by two-way ANOVA with Holm–Sidak correction. **B,** Mouse survival for each treatment group. Treatment windows indicate when mice were treated. Significance calculated using Mantel–Cox tests. **C,** Waterfall plot of vehicle and idasanutlin-treated tumors at day 11. *Y*-axes represent the fold change in tumor volume on a $\log_2$ scale (left) and percent change in tumor volume (right). Each bar represents one tumor. Significance calculated with a two-sided *t* test. **D,** Individual mouse tumor volumes for the vehicle and idasanutlin groups. **E,** Quantitation of Ki-67$^+$ cells from tumors shown in Supplementary Fig. S7F–S7H. Data show mean ± SD of three independent tumors. Significance calculated by one-way ANOVA with Holm–Sidak multiple comparisons correction. **F,** Immunoblot showing p53 pathway response to idasanutlin and ATSP-7041 treatment in mice bearing TTC642 xenografts. Three independent tumors are shown for each condition. **, $P < 0.01$; ***, $P < 0.001$; ****, $P < 0.0001$.

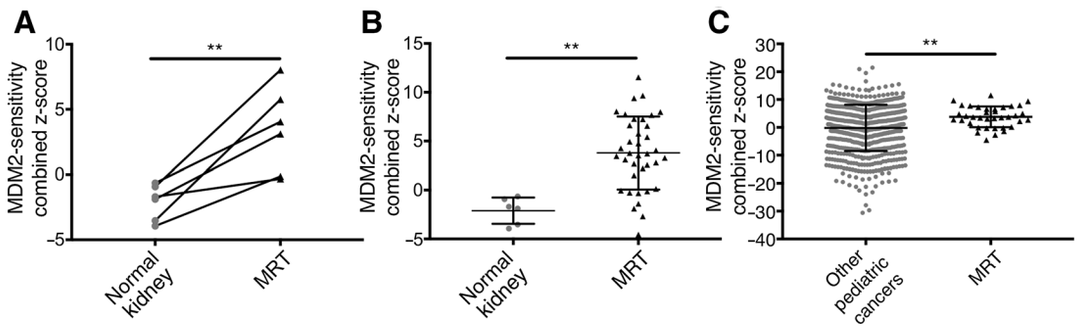

Figure 7.

Primary MRTs are predicted to be sensitive to MDM2 inhibition. **A,** Predictive scores for MDM2 inhibitor sensitivity in six normal kidney samples and their matched primary MRT pairs. MDM2 sensitivity score calculated as the sum of *z*-score expression levels of thirteen p53 target genes. Higher scores indicate greater predicted sensitivity. Significance calculated with a two-sided paired *t* test. **B,** Predictive scores for MDM2 inhibitor sensitivity in six normal kidney samples and 37 primary MRT samples. Data show mean ± SD. Significance calculated with a two-sided *t* test. **C,** Predictive scores for MDM2 inhibitor sensitivity between 656 pediatric tumors and 37 primary MRT samples. Data show mean ± SD. Significance calculated with a two-sided *t* test. **, $P < 0.01$.

We found that primary MRTs were predicted to be significantly more sensitive to MDM2 inhibition than their normal kidney pairs ($P = 0.0070$; Fig. 7A and B) and other pediatric cancers ($P = 0.0039$; Fig. 7C). Together, these data suggest that primary MRTs, like cell lines and xenografts, are likely to be sensitive to MDM2 inhibition.

Discussion

Given the lack of actionable mutations and very poor prognoses in MRTs, new therapies are urgently needed. In this study, we report the convergence of large-scale RNAi, CRISPR-Cas9, and small-molecule screens across 8 to 10 MRT cell lines on *MDM2* and *MDM4* as actionable targets. Both idasanutlin and ATSP-7041 showed potent, on-target activity *in vitro* and *in vivo* against MRTs. Although idasanutlin alone created durable complete responses in some mice, our assays were not designed to directly compare the compounds *in vivo* as the dosages, schedules, and routes of exposure varied. In addition, unlike idasanutlin, ATSP-7041 is not the exact compound used in patients. Further work is needed to fully optimize a potential dosing schedule and formulation of both clinical compounds in children. The Pediatric Preclinical Testing Program investigated an earlier generation MDM2 inhibitor (RG7112) across many types of pediatric cancer, and also saw activity against MRTs (37). Thus, idasanutlin, ATSP-7041, or one of the multiple other compounds in development targeting negative regulators of p53, including MDM2, MDM4, PPM1D, and USP7, could feasibly be redirected toward a trial in MRTs.

The SWI/SNF chromatin-remodeling complex, originally discovered in yeast, has long been known to facilitate transcriptional regulation and the function of transcription factors (38). p53 itself is a transcription factor, and multiple studies have reported both physical interactions between SWI/SNF and p53 as well as contributions of SWI/SNF to p53 transcriptional function (31, 39–43). Notably, we find in MRT cells that activation of p53 via MDM2 and MDM2/4 inhibition results in differential effects depending upon the presence of SMARCB1. In the unmodified TTC642 cell line, activation of p53 triggers a marked increase in cleaved caspase-3, indicative of an apoptotic response, while reexpression of SMARCB1 fully eliminates this effect but leaves intact the upregulation of p21, consistent with a cell-cycle arrest phenotype. We and others have recently demonstrated that SMARCB1 enables targeting of SWI/SNF to enhancers where the complex facilitates enhancer function and expression of differentiation-associated genes (10, 11). Consequently, one explanation for the differential effects of MDM2 and MDM2/4 inhibition in the presence of SMARCB1 in MRT cells is an inhibition of global p53 responses following cell differentiation triggered by SMARCB1. Multiple context-specific effects for p53 in development and differentiation have been reported, with the specific cell type and context determining the output of the p53 pathway (44). A second possibility is that the functional, SMARCB1-proficient SWI/SNF complex changes the chromatin landscape at a subset of p53 target genes, thereby directly influencing the ability of p53 to bind and activate transcription, and favoring an arrest outcome rather than apoptosis. Further studies are needed to fully elucidate how SMARCB1 influences p53-mediated gene expression at the chromatin level and how these transcriptional effects are integrated to dictate cell fate following p53 activation.

One potential confounder to the experiments linking idasanutlin sensitivity to *SMARCB1* is that reexpression of SMARCB1 itself impairs cell-cycle progression in MRT cell lines (31, 42). This arrest is at least partially mediated by increased expression of p21, which can be induced by both p53-dependent and -independent mechanisms in MRT cell lines (42). We show that expressing $p16^{INK4A}$ did not impact sensitivity to these compounds, providing evidence that the observed resistance is not simply due to changes in proliferation. Furthermore, at least in the TTC642 cells used here, SMARCB1 reexpression on its own does not activate p21 through the p53 pathway (42). Thus, the differential responses to idasanutlin with and without SMARCB1 reflect alterations in idasanutlin-mediated p53 pathway activation rather than p53 activation by SMARCB1 itself.

An additional outstanding question is whether these findings extend to cancers with mutations in other subunits of the SWI/SNF complex. Notably A549, the p53 WT cell line that was most sensitive to MDM2 and MDM2/4 inhibition in this study, harbors a mutation in *SMARCA4*, the SWI/SNF subunit that is lost in the small minority of MRTs that retain *SMARCB1* (45). Future experiments would be necessary to determine whether this observation reflects a wider connection between SWI/SNF mutations sensitizing cells to p53 activation.

The findings reported here provide another functional and clinically actionable link between p53 and the SWI/SNF complex, two of the most frequently mutated tumor suppressors. Virtually, all MRTs in patients retain WT *TP53* (5, 6, 8) with a marked paucity of mutations other than SMARCB1 loss, and primary MRTs express a gene expression signature associated with p53 pathway activity and MDM2 inhibitor sensitivity. A pristine p53 pathway with augmentation of dependence upon MDM2/4 mediated by SMARCB1 loss may make MRTs an ideal target for these experimental cancer therapies.

Disclosure of Potential Conflicts of Interest

A. Tsherniak is a consultant/advisory board member for Tango Therapeutics. K. Stegmaier reports receiving a commercial research grant from Novartis. L.D. Walensky is a consultant/advisory board member for Aileron Therapeutics and has ownership interest (including stocks and patents) in Aileron Therapeutics. W.C. Hahn reports receiving a commercial research grant from Deerfield, has ownership interest (including stocks and patents) in KSQ Therapeutics, and is a consultant/advisory board member for Thermo Fisher Scientific, Paraxel, AjuIB, KSQ Therapeutics, and MPM. No potential conflicts of interest were disclosed by the other authors.

Authors' Contributions

Conception and design: T.P. Howard, A.O. Giacomelli, F. Vazquez, K.H. Walsh, P.C. Gokhale, K. Stegmaier, W.C. Hahn, C.W.M. Roberts

Development of methodology: T.P. Howard, T.E. Arnoff, A.L. Hong, F. Vazquez, J.H. Hwang, A. Cook, J.M. Krill-Burger, A. Tsherniak, L.D. Walensky, C.W.M. Roberts

Acquisition of data (provided animals, acquired and managed patients, provided facilities, etc.): T.P. Howard, T.E. Arnoff, M.R. Song, F. Vazquez, M.-T. Pham, A.M. Morgan, F. Wachter, G.H. Bird, H.L. Tiv, J.H. Hwang, P.C. Gokhale,

Analysis and interpretation of data (e.g., statistical analysis, biostatistics, computational analysis): T.P. Howard, T.E. Arnoff, X. Wang, N.V. Dharia, S. Wang, F. Vazquez, M.-T. Pham, G. Kugener, E.M. Oberlick, M.G. Rees, H.L. Tiv, A. Tsherniak, P.C. Gokhale, P.J. Park, L.D. Walensky, W.C. Hahn, C.W.M. Roberts

Writing, review, and/or revision of the manuscript: T.P. Howard, T.E. Arnoff, M.R. Song, A.O. Giacomelli, X. Wang, A.L. Hong, N.V. Dharia, F. Vazquez, M.-T. Pham, G. Kugener, M.G. Rees, J.H. Hwang, A. Cook, A. Tsherniak, K. Stegmaier, L.D. Walensky, W.C. Hahn, C.W.M. Roberts

Administrative, technical, or material support (i.e., reporting or organizing data, constructing databases): T.P. Howard, T.E. Arnoff, X. Wang, A.L. Hong, W.C. Hahn,

Study supervision: K. Stegmaier, W.C. Hahn, C.W.M. Roberts

Acknowledgments

The authors thank the Roberts, Hahn, and Cichowski labs, and Pediatric Dependencies Project for insightful discussions. The authors thank Roche for providing formulated idasanutlin for *in vivo* studies, Daniel Bauer for advice on sgRNA design, and Sayalee Potdar and Jake Kloeber for assistance with Illumina sequencing. The authors thank John Daley for assistance with flow cytometry and Franck Bordeaut, Yoon-Jae Cho, C. David James, Yasumichi Kuwahara, Timothy Triche, Geoffrey Wahl, and Bernard Weissman for cell lines. This work was supported by U.S. NIH grants T32GM007753 (to T.P. Howard and A.M. Morgan), T32GM007226 (to T.P. Howard), R00CA197640 (to X. Wang), P50CA101942 (to A.L. Hong), T32CA136432 (to N.V. Dharia), F30CA221087 (to A.M. Morgan), 1R50CA211399 (to G.H. Bird), R35CA210030 (to K. Stegmaier), U01CA176058 (to W.C. Hahn), R01CA172152 (to C.W.M. Roberts), and R01CA113794 (to C.W.M. Roberts); ACS Mentored Research Scholar Grant 132943-MRSG-18-202-01-TBG (to A.L. Hong), St. Baldrick's Robert J. Arceci Award (to K. Stegmaier), Hyundai Hope on Wheels Quantum Award (to L.D. Walensky), Alex's Lemonade Stand REACH Grant (to L.D. Walensky), Cure AT/RT Now (to C.W.M. Roberts), Avalanna Fund (to C.W. M. Roberts), Garrett B. Smith Foundation (to C.W.M. Roberts), and ALSAC/St. Jude (to C.W.M. Roberts). This work is partially based upon data generated by the Cancer Target Discovery and Development (CTD2) Network (https://ocg.cancer.gov/programs/ctd2/data-portal) and the TARGET initiative (http://ocg.cancer.gov/programs/target).

The costs of publication of this article were defrayed in part by the payment of page charges. This article must therefore be hereby marked *advertisement* in accordance with 18 U.S.C. Section 1734 solely to indicate this fact.

Received October 1, 2018; revised December 28, 2018; accepted February 7, 2019; published first February 12, 2019.

References

1. Dome JS, Fernandez CV, Mullen EA, Kalapurakal JA, Geller JI, Huff V, et al. Children's Oncology Group's 2013 blueprint for research: renal tumors. Pediatr Blood Cancer 2013;60:994–1000.
2. Bartelheim K, Nemes K, Seeringer A, Kerl K, Buechner J, Boos J, et al. Improved 6-year overall survival in AT/RT - results of the registry study Rhabdoid 2007. Cancer Med 2016;5:1765–75.
3. Fischer-Valuck BW, Chen I, Srivastava AJ, Floberg JM, Rao YJ, King AA, et al. Assessment of the treatment approach and survival outcomes in a modern cohort of patients with atypical teratoid rhabdoid tumors using the National Cancer Database. Cancer 2017;123:682–7.
4. Roberts CW, Biegel JA. The role of SMARCB1/INI1 in development of rhabdoid tumor. Cancer Biol Ther 2009;8:412–6.
5. Kieran MW, Roberts CW, Chi SN, Ligon KL, Rich BE, Macconaill LE, et al. Absence of oncogenic canonical pathway mutations in aggressive pediatric rhabdoid tumors. Pediatr Blood Cancer 2012;59:1155–7.
6. Lee RS, Stewart C, Carter SL, Ambrogio L, Cibulskis K, Sougnez C, et al. A remarkably simple genome underlies highly malignant pediatric rhabdoid cancers. J Clin Invest 2012;122:2983–8.
7. Torchia J, Picard D, Lafay-Cousin L, Hawkins CE, Kim SK, Letourneau L, et al. Molecular subgroups of atypical teratoid rhabdoid tumours in children: an integrated genomic and clinicopathological analysis. Lancet Oncol 2015;16:569–82.
8. Johann PD, Erkek S, Zapatka M, Kerl K, Buchhalter I, Hovestadt V, et al. Atypical teratoid/rhabdoid tumors are comprised of three epigenetic subgroups with distinct enhancer landscapes. Cancer Cell 2016;29:379–93.
9. Roberts CW, Leroux MM, Fleming MD, Orkin SH. Highly penetrant, rapid tumorigenesis through conditional inversion of the tumor suppressor gene Snf5. Cancer Cell 2002;2:415–25.
10. Wang X, Lee RS, Alver BH, Haswell JR, Wang S, Mieczkowski J, et al. SMARCB1-mediated SWI/SNF complex function is essential for enhancer regulation. Nat Genet 2017;49:289–95.
11. Nakayama RT, Pulice JL, Valencia AM, McBride MJ, McKenzie ZM, Gillespie MA, et al. SMARCB1 is required for widespread BAF complex-mediated activation of enhancers and bivalent promoters. Nat Genet 2017;49:1613–23.
12. Wilson BG, Wang X, Shen X, McKenna ES, Lemieux ME, Cho YJ, et al. Epigenetic antagonism between polycomb and SWI/SNF complexes during oncogenic transformation. Cancer Cell 2010;18:316–28.
13. Kim KH, Kim W, Howard TP, Vazquez F, Tsherniak A, Wu JN, et al. SWI/SNF-mutant cancers depend on catalytic and non-catalytic activity of EZH2. Nat Med 2015;21:1491–6.
14. Kadoch C, Williams RT, Calarco JP, Miller EL, Weber CM, Braun SM, et al. Dynamics of BAF-Polycomb complex opposition on heterochromatin in normal and oncogenic states. Nat Genet 2017;49:213–22.
15. Kim KH, Roberts CW. Mechanisms by which SMARCB1 loss drives rhabdoid tumor growth. Cancer Genet 2014;207:365–72.
16. Wade M, Li YC, Wahl GM. MDM2, MDMX and p53 in oncogenesis and cancer therapy. Nat Rev Cancer 2013;13:83–96.
17. Pant V, Xiong S, Iwakuma T, Quintas-Cardama A, Lozano G. Heterodimerization of Mdm2 and Mdm4 is critical for regulating p53 activity during embryogenesis but dispensable for p53 and Mdm2 stability. Proc Natl Acad Sci U S A 2011;108:11995–2000.

18. Tsherniak A, Vazquez F, Montgomery PG, Weir BA, Kryukov G, Cowley GS, et al. Defining a cancer dependency map. Cell 2017;170: 564–76.
19. Sanjana NE, Shalem O, Zhang F. Improved vectors and genome-wide libraries for CRISPR screening. Nat Methods 2014;11:783–4.
20. Aguirre AJ, Meyers RM, Weir BA, Vazquez F, Zhang CZ, Ben-David U, et al. Genomic copy number dictates a gene-independent cell response to CRISPR/Cas9 targeting. Cancer Discov 2016;6:914–29.
21. Giacomelli AO, Yang X, Lintner RE, McFarland JM, Duby M, Kim J, et al. Mutational processes shape the landscape of TP53 mutations in human cancer. Nat Genet 2018;50:1381–7.
22. Seashore-Ludlow B, Rees MG, Cheah JH, Cokol M, Price EV, Coletti ME, et al. Harnessing connectivity in a large-scale small-molecule sensitivity dataset. Cancer Discov 2015;5:1210–23.
23. Rees MG, Seashore-Ludlow B, Cheah JH, Adams DJ, Price EV, Gill S, et al. Correlating chemical sensitivity and basal gene expression reveals mechanism of action. Nat Chem Biol 2016;12:109–16.
24. Bird GH, Crannell WC, Walensky LD. Chemical synthesis of hydrocarbon-stapled peptides for protein interaction research and therapeutic targeting. Curr Protoc Chem Biol 2011;3:99–117.
25. Chang YS, Graves B, Guerlavais V, Tovar C, Packman K, To KH, et al. Stapled alpha-helical peptide drug development: a potent dual inhibitor of MDM2 and MDMX for p53-dependent cancer therapy. Proc Natl Acad Sci U S A 2013;110:E3445–54.
26. Heigwer F, Kerr G, Boutros M. E-CRISP: fast CRISPR target site identification. Nat Methods 2014;11:122–3.
27. Bauer DE, Canver MC, Orkin SH. Generation of genomic deletions in mammalian cell lines via CRISPR/Cas9. J Vis Exp. 2015:e52118.
28. Stolte B, Iniguez AB, Dharia NV, Robichaud AL, Conway AS, Morgan AM, et al. Genome-scale CRISPR-Cas9 screen identifies druggable dependencies in TP53 wild-type Ewing sarcoma. J Exp Med 2018;215: 2137–55.
29. Chun HE, Lim EL, Heravi-Moussavi A, Saberi S, Mungall KL, Bilenky M, et al. Genome-wide profiles of extra-cranial malignant rhabdoid tumors reveal heterogeneity and dysregulated developmental pathways. Cancer Cell 2016;29:394–406.
30. Jeay S, Gaulis S, Ferretti S, Bitter H, Ito M, Valat T, et al. A distinct p53 target gene set predicts for response to the selective p53-HDM2 inhibitor NVP-CGM097. Elife 2015;4. doi: 10.7554/eLife.06498.
31. Chai J, Charboneau AL, Betz BL, Weissman BE. Loss of the hSNF5 gene concomitantly inactivates p21CIP/WAF1 and p16INK4a activity associated with replicative senescence in A204 rhabdoid tumor cells. Cancer Res 2005; 65:10192–8.
32. Ding Q, Zhang Z, Liu JJ, Jiang N, Zhang J, Ross TM, et al. Discovery of RG7388, a potent and selective p53-MDM2 inhibitor in clinical development. J Med Chem 2013;56:5979–83.
33. Barretina J, Caponigro G, Stransky N, Venkatesan K, Margolin AA, Kim S, et al. The Cancer Cell Line Encyclopedia enables predictive modelling of anticancer drug sensitivity. Nature 2012;483:603–7.
34. Venneti S, Le P, Martinez D, Eaton KW, Shyam N, Jordan-Sciutto KL, et al. p16INK4A and p14ARF tumor suppressor pathways are deregulated in malignant rhabdoid tumors. J Neuropathol Exp Neurol 2011;70:596–609.
35. Fischer M. Census and evaluation of p53 target genes. Oncogene 2017;36: 3943–56.
36. Subramanian A, Tamayo P, Mootha VK, Mukherjee S, Ebert BL, Gillette MA, et al. Gene set enrichment analysis: a knowledge-based approach for interpreting genome-wide expression profiles. Proc Natl Acad Sci U S A 2005;102:15545–50.
37. Carol H, Reynolds CP, Kang MH, Keir ST, Maris JM, Gorlick R, et al. Initial testing of the MDM2 inhibitor RG7112 by the Pediatric Preclinical Testing Program. Pediatr Blood Cancer 2013;60:633–41.
38. Sudarsanam P, Winston F. The Swi/Snf family nucleosome-remodeling complexes and transcriptional control. Trends Genet 2000;16:345–51.
39. Lee D, Kim JW, Seo T, Hwang SG, Choi EJ, Choe J. SWI/SNF complex interacts with tumor suppressor p53 and is necessary for the activation of p53-mediated transcription. J Biol Chem 2002;277:22330–7.
40. Klochendler-Yeivin A, Picarsky E, Yaniv M. Increased DNA damage sensitivity and apoptosis in cells lacking the Snf5/Ini1 subunit of the SWI/SNF chromatin remodeling complex. Mol Cell Biol 2006;26:2661–74.
41. Oh J, Sohn DH, Ko M, Chung H, Jeon SH, Seong RH. BAF60a interacts with p53 to recruit the SWI/SNF complex. J Biol Chem 2008;283:11924–34.
42. Kuwahara Y, Charboneau A, Knudsen ES, Weissman BE. Reexpression of hSNF5 in malignant rhabdoid tumor cell lines causes cell cycle arrest through a p21(CIP1/WAF1)-dependent mechanism. Cancer Res 2010;70: 1854–65.
43. Kuwahara Y, Wei D, Durand J, Weissman BE. SNF5 reexpression in malignant rhabdoid tumors regulates transcription of target genes by recruitment of SWI/SNF complexes and RNAPII to the transcription start site of their promoters. Mol Cancer Res 2013;11:251–60.
44. Molchadsky A, Rivlin N, Brosh R, Rotter V, Sarig R. p53 is balancing development, differentiation and de-differentiation to assure cancer prevention. Carcinogenesis 2010;31:1501–8.
45. Schneppenheim R, Fruhwald MC, Gesk S, Hasselblatt M, Jeibmann A, Kordes U, et al. Germline nonsense mutation and somatic inactivation of SMARCA4/BRG1 in a family with rhabdoid tumor predisposition syndrome. Am J Hum Genet 2010;86:279–4.